Understanding the Regional Variability of Eddy Diffusivity in the Pacific Sector of the Southern Ocean

EMILY SHUCKBURGH

British Antarctic Survey, Cambridge, United Kingdom

HELEN JONES, JOHN MARSHALL, AND CHRIS HILL

Department of Earth, Atmospheric and Planetary Sciences, Massachusetts Institute of Technology, Cambridge, Massachusetts

(Manuscript received 8 August 2008, in final form 23 February 2009)

ABSTRACT

A diagnostic framework is presented, based on the Nakamura effective diffusivity, to investigate the regional variation in eddy diffusivity. Comparison of three different diffusivity calculations enables the effects of locally enhanced tracer diffusion to be distinguished from the streamwise average. It also enables the distinction to be made between locally generated complexity in the tracer structure and that advected into a particular domain. The technique is applied to the Pacific sector of the Southern Ocean. The results highlight the important role that the mean flow plays in determining eddy diffusivity. The effective diffusivity is not simply related to the eddy kinetic energy: in regions of a strong mean flow the eddy diffusivity can be suppressed even in the presence of moderately strong eddy activity; conversely, in a region of weak mean flow the eddy diffusivity can be enhanced even in the presence of only weak eddy activity. This casts doubt on the ability of parameterizations based solely on the eddy kinetic energy to adequately characterize the eddy diffusivity in regions of strongly varying mean flow such as the Southern Ocean. The results are, however, consistent with the eddy transport and mixing variability predicted by potential-vorticity-based arguments.

1. Introduction

Throughout the ocean, satellite altimetry data reveal a complex regional eddy kinetic energy (EKE) distribution (Stammer 1997; Stammer et al. 2006). Significant enhancement in eddy activity is observed in the vicinity of strong currents: the Gulf Stream in the Atlantic, the Kuroshio and its extension in the Pacific, and the Antarctic Circumpolar Current (ACC) in the Southern Ocean. Much of this eddy activity arises through baroclinic instability, although barotropic instability, wind forcing, and topographic interactions are also thought to play a role in some regions. In addition there is strong variability in the strength of the eddy activity along these currents. Treguier et al. (2007) note that in both observations and modeling studies the EKE varies by a factor of more than 10 along the path of the ACC, with particularly large values in the regions of the East Australia Current, the Southwest Indian Ridge, the Brazil–Malvinas confluence, and the Agulhas Retroflection (see also, e.g., Gille 1997).

Eddies are known to play a particularly important role in the dynamics of the Southern Ocean, a region where the water masses of much of the global ocean are either formed, modified, or transit (Hallberg and Gnandesikan 2006 and references therein). The residual-mean framework of Marshall and Radko (2003) relates the eddy diffusivity to the strength of the overturning circulation and to the baroclinic transport of the ACC. A recent study (Williams et al. 2007) has emphasized the dynamical consequences of the along-stream eddy variability and likened it to the atmospheric storm tracks where eddies grow in the entrance region, providing a downgradient tracer flux accelerating the flow eastward, and decay in the exit region, with the opposite effects. Satellite data and in situ observations (e.g., Lenn et al. 2007) have shown that the ACC comprises

Corresponding author address: Emily Shuckburgh, British Antarctic Survey, High Cross, Madingley Road, Cambridge, CB3 0ET, United Kingdom.
E-mail: emsh@bas.ac.uk

DOI: 10.1175/2009JPO4115.1

multiple jets (Hughes and Ash 2001) that merge and diverge along the circumpolar path [these jets appear to be consistently aligned with particular streamlines resulting in the distinct fronts seen in hydrographic data, Sokolov and Rintoul (2007)]. The alignment of the jets is clearly influenced in places by topography and associated eddy–mean flow interactions (Hughes and Ash 2001). Williams et al. (2007) point out that meanders in the Antarctic Circumpolar Current have a dominant wavelength of 300–500 km, consistent with the Rhines scale (Rhines 1975), and that the separation between this scale and the scale of eddies in the Southern Ocean (~30 km) allows the eddies to become organized with respect to such variations of the mean flow.

To properly parameterize the behavior of eddies in coarse-resolution climate models, an understanding of the influence on the large-scale ocean dynamics of this regional eddy variation is necessary, together with a description of the physical mechanisms generating it. The results of the modeling study of Treguier et al. (2007) highlight the need to take into account along-stream variations to understand the Southern Ocean overturning circulation and its relation to surface forcing. Sallée et al. (2008) considers subantarctic mode water, which is formed in deep winter mixed layers directly north of the Subantarctic Front. They note that the action of Ekman fluxes and air–sea interaction in destabilization of the mixed layer, during which the mode water is renewed, can be modified locally by eddy heat fluxes.

Here we will attempt to gain a clearer understanding of one aspect of this eddy variability—the regional changes in near-surface eddy diffusivity. All results to be presented here will be from the Pacific sector of the Southern Ocean. In this region, with a rich eddy field and a strong mean flow, there are complex and poorly understood interactions between eddies and the mean flow, and an apparently strong influence of bathymetry (Hallberg and Gnandesikan 2001; Hughes and Ash 2001; Stammer et al. 2006), which may be expected to lead to strong spatial variations in the eddy diffusivity. Shuckburgh et al. (2009b), found that meridional and temporal variations in the eddy diffusivity are related to variations in the EKE, mean zonal current (u), and phase speed (c) of the eddies, scaling with the streamwise average of $\mathrm{EKE}/(u-c)^2$. The relationship between these flow parameters and the effective diffusivity will be explored in further detail here; in particular, we will examine whether the relationship between effective diffusivity and $\mathrm{EKE}/(u-c)^2$ holds regionally.

Existing information regarding regional eddy diffusivities is somewhat unsatisfactory. Holloway (1986) (see also Keffer and Holloway 1988; Stammer 1998; Karsten and Marshall 2002) used sea surface height (SSH) anomalies from altimetry to derive an eddy diffusivity. However, this diffusivity is only defined up to a constant of proportionality, and it can be biased by the inclusion of large-scale features not related to eddy activity (see Shuckburgh et al. 2009b). Moreover, it does not take into account the potentially important impact of the mean flow on the eddy diffusivity. Lagrangian particle diagnostics such as finite-time Lyapunov exponents (FTLEs) have been used to determine the horizontal mixing structure of ocean surface flows (Waugh et al. 2006); however, it is not yet clear how to relate these diagnostics to an eddy diffusivity. Direct observational data comes from moorings, floats, and drifters, but there are fundamental problems associated with the interpretation of such data in the context of deriving eddy diffusivities (Marshall et al. 2006).

The paper is organized as follows. First, we outline the diagnostic approach, introducing two new eddy diffusivity calculations aimed at better understanding along-stream variability (section 2). Then, we apply these diagnostics to the southeastern sector of the Pacific, with a particular focus on the regions of the Chatham Rise; the Eltanin, Udinstev and Menard Fracture Zones; and the deep ocean basin (section 3). Finally, we consider some of the temporal variability (section 4) in the Pacific region.

2. Diagnostic approach

a. Effective diffusivity calculation

We will use the effective diffusivity diagnostic of Nakamura (1996) (see also Shuckburgh and Haynes 2003; Marshall et al. 2006; Shuckburgh et al. 2009b) to provide information concerning the cross-stream eddy diffusivities in the Southern Ocean. We use a velocity field derived from altimetric observations, which is representative of the surface geostrophic flow, to advect a tracer at $1/20°$ resolution using the Massachusetts Institute of Technology general circulation model (Marshall et al. 1997) in an offline mode. The tracer is initialized to be aligned with the mean streamlines on 30 December 1996 and a 3-month spinup is allowed before calculation of the effective diffusivity. The tracer integration is continued for one year. A value of numerical diffusion of $k = 50\ \mathrm{m^2\ s^{-1}}$ is used following Marshall et al. (2006) and Shuckburgh et al. (2009b).

Extensive use is made in this paper of calculations on small patches of the ocean, typically 20° longitude across. Owing to their relative computational efficiency, Marshall et al. (2006) made use of such patch calculations to assess the sensitivity of the effective diffusivity calculation to the value of numerical diffusion. Here we use the patches as a basis for examining regional

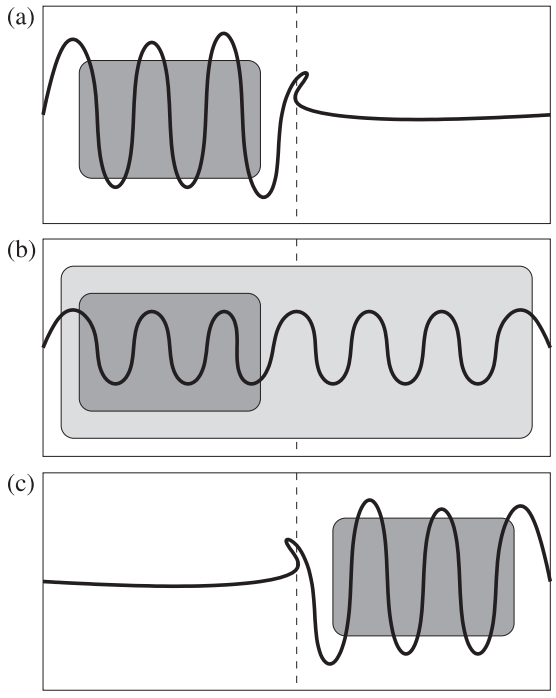

FIG. 1. Schematic indicating three possible tracer contour configurations that could result in the same equivalent length. Three possible mixing scenarios may occur: (a),(c) (i) localized mixing in part of the domain (dark gray shading) resulting in locally complex tracer contours; (b) (ii) localized mixing in part of the domain, resulting in complex structure in the tracer contours that is then advected to other parts of the domain; and (iii) mixing throughout the domain (light gray shading) resulting in complex tracer contours throughout the domain [also (b)].

variability of the eddy diffusivity. The velocity field used for these patch calculations is modified slightly to create a reentrant channel that is periodic in longitude and has no flow out of the north and south boundaries. The zonal mean of the mean streamfunction is used, and for this reason the patches are chosen in regions across which the mean streamlines are predominantly zonal (were this technique to be used in other regions of the ocean where this is not the case, it would be sensible to orient the patch such that it is aligned with the predominant direction of the mean streamlines). The SSH anomalies for the patch are obtained and for each latitude the Fourier transform is taken and the largest wavenumbers discarded. Sensitivity studies outlined in Shuckburgh et al. (2009b) indicated that the largest wavenumbers in the velocity field do not contribute significantly to the tracer structure (nor to the effective diffusivity). Removal of the largest wavenumbers acts to smooth the step associated with the east and west boundaries of the patch. A longitudinally periodic SSH field is then obtained by taking the inverse Fourier transform; from this and the mean streamfunction the velocity field is derived, as described in Shuckburgh et al. (2009b).

b. Along-stream variations in eddy diffusivity

One of the disadvantages of the effective diffusivity approach is that it does not provide local information, being a streamwise-average quantity. However, calculations based on subregions of the domain of interest may be used to deduce some local information concerning the along-stream variations. Figure 1 illustrates three possible tracer contour configurations that could result in similar large values of κ_{eff}. In the first case (Fig. 1a), the large κ_{eff} is a consequence of strong mixing (represented by the gray shading) occurring in the left box, but not in the right box. The strong mixing creates a complex tracer contour in the left box whereas in the right box the tracer contour remains simple. The opposite is true in the third case (Fig. 1c). In the second case (Fig. 1b), the tracer contour has a similar moderately complex structure across the region. This may arise either from moderate mixing throughout the region (the light gray shading) or from mixing in the left box that creates a moderately complex tracer structure, which is then advected into the right box.

Here we introduce two additional calculations to help distinguish between the different scenarios for a patch of the Pacific. First, the effective diffusivity is calculated from the tracer field from the full Southern Ocean simulation, cropped to the patch of interest.[1] The results of this calculation are denoted $\kappa_{\mathrm{eff}}^{>}$. Large values of $\kappa_{\mathrm{eff}}^{>}$ must be due to complex tracer contours in the patch region itself, but that complex tracer structure may have arisen elsewhere and then been advected into the patch. In terms of the schematic in Fig. 1, if the patch is the right-hand square, then the values of $\kappa_{\mathrm{eff}}^{>}$ in scenario b may or may not be a result of local mixing. Second, a patch calculation is performed using a tracer field simulated using the velocity field only from the patch, made periodic in the manner described above.[2] From this tracer field the local effective diffusivity $\kappa_{\mathrm{eff}}^{\#}$ is calculated. Large values of $\kappa_{\mathrm{eff}}^{\#}$ must be due to local mixing processes. The eddies themselves may have been generated by instability processes elsewhere and advected into the region to contribute to the SSH anomalies, but the tracer structure must be locally generated. In terms

[1] Such a calculation is not mathematically rigorous in the sense that, considering the derivation of the effective diffusivity (Nakamura 1996; Shuckburgh et al. 2001), the area between tracer contours within this cropped domain can change for reasons other than irreversible mixing. Here, therefore, we consider the $\kappa_{\mathrm{eff}}^{>}$ to be a characterization of the complexity of the tracer contours in the cropped domain, rather than an exact quantification of the eddy diffusivity.

[2] Patches of no more than 20° longitude are used. Over this longitude range the mean streamlines do not vary substantially in latitude and hence the effect of taking the zonal mean is limited.

of the right-hand square in Fig. 1, scenario a would give small values of $\kappa^{\#}_{\rm eff}$, scenario c would give large values, and the two possible causes of the tracer structure in scenario b would be distinguished.

This approach is tested in Fig. 2 for patches in the Pacific from 38° to 59°S, 180° to 80°W. The black solid curve shows the results of the calculation of $\kappa^{>}_{\rm eff}$ for this region and the black dotted curve shows the streamwise average of five patches, each 20° in longitude covering the same region. Although the streamwise average shows less small-scale variability, the larger-scale variations of the two curves are similar, providing some confidence in the robustness of the technique. The red curve shows $\kappa_{\rm eff}$ for the full Southern Ocean $\kappa_{\rm eff}$ at these equivalent latitudes. There is broad similarity between this and $\kappa^{>}_{\rm eff}$, except in the region 48°–46°. The blue curve shows the streamwise average of $\kappa^{\#}_{\rm eff}$ for the same five 20° longitude patches as the black dotted curve. There is very close agreement between the two results equatorward of 50°. Poleward of this, the values of $\kappa^{\#}_{\rm eff}$ are higher than the other effective diffusivities. This may indicate that there is significant local mixing in this region that has been enhanced by the periodic flow used in the calculation of $\kappa^{\#}_{\rm eff}$.

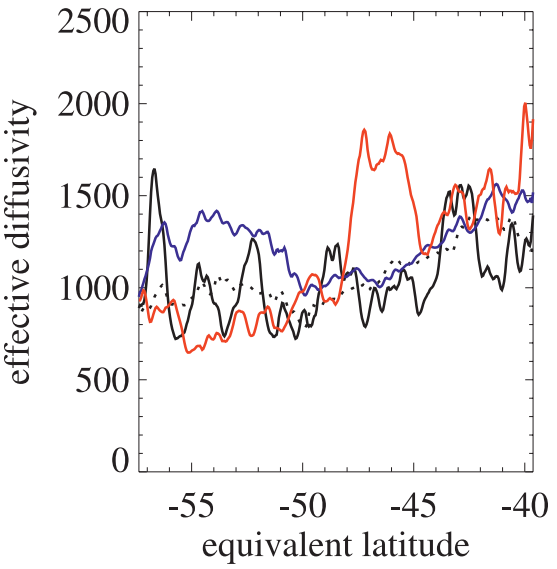

FIG. 2. Effective diffusivity from four different calculations: $\kappa_{\rm eff}$ (red solid), $\kappa^{>}_{\rm eff}$ for a patch in the Pacific from 38° to 59°S, 180° to 80°W (black solid); streamwise average of $\kappa^{>}_{\rm eff}$ for five patches, each 20° longitude covering the same Pacific patch (black dotted); and streamwise average of $\kappa^{\#}_{\rm eff}$ for the same five patches (blue solid).

3. Regional variability of eddy diffusivity in the Pacific sector

a. Eltanin and Udinstev Fracture Zones

Figure 3 presents the results of the three eddy diffusivity calculations in a patch of the Pacific from 38° to 59°S, 160° to 140°W. The first panel in Fig. 3 shows a patch of the full Southern Ocean $\kappa_{\rm eff}$ calculation. There are high values of diffusivity (>2000 m^2 s^{-1}) to the north of the domain with smaller values to the south (<1000 m^2 s^{-1}). The second panel shows the effective diffusivity calculated from the tracer field restricted to the patch of interest, $\kappa^{>}_{\rm eff}$. There is little difference between the values of $\kappa_{\rm eff}$ and $\kappa^{>}_{\rm eff}$ in the northern half of the domain. In the southern half of the domain, the $\kappa^{>}_{\rm eff}$ values are up to half the $\kappa_{\rm eff}$ values, indicating that this region is rather quiescent compared to other longitudes. It is interesting to note that there is a clearly defined minimum in $\kappa^{>}_{\rm eff}$, which follows the instantaneous zero geostrophic streamline closely (white dots), and another local minimum just south of this that also follows an instantaneous streamline. These minima are associated with eastward jets in the flow (see Fig. 4c). Considering the $\kappa^{\#}_{\rm eff}$ results, it can be seen that in the northern half of the domain the values are considerably reduced compared to $\kappa^{>}_{\rm eff}$ and $\kappa_{\rm eff}$. These results might indicate that the large values of $\kappa_{\rm eff}$ in the northern half of the domain are predominantly a result of mixing outside the domain, generating complex structure in the tracer contours that is then advected into the patch. However, the fact that the time-mean streamlines exhibit considerable longitudinal asymmetries in this region and the $\kappa^{\#}_{\rm eff}$ calculation uses the zonal mean of this complicates the interpretation in this region. In the southern half of the domain the values of $\kappa^{\#}_{\rm eff}$ are similar to those of $\kappa^{>}_{\rm eff}$ with the exception of a few small regions of $\kappa^{\#}_{\rm eff} > 2000$ m^2 s^{-1}. These results suggest that there is some localized enhanced mixing in the southern half of the patch, but that this is overwhelmed by the effects of advection from other regions in the case of $\kappa^{>}_{\rm eff}$. Looking to the details of the mixing structure in Fig. 3c, there is evidence of a pattern very similar to the idealized chaotic advection studies of Shuckburgh and Haynes (2003); for example, compare the eddy feature at approximately 52°S, 145°W with their Fig. 3.

Figure 4 presents results that seek to further understand those of Fig. 3. From the SSH anomalies (Fig. 4a), it can be seen that the greatest eddy activity appears to be in the region of the ACC jet, around the zero streamfunction contour. Figure 4c presents the bathymetry for the patch from version 8.2 of the Smith and Sandwell (1997) dataset. The Polar and Subantarctic Fronts are observed to pass along the Udinstev Fracture Zone[3] as the jets in the flow are steered by the topography (e.g.,

[3] The Udinstev Fracture Zone is visible in Fig. 4c entering the domain at 50°S, 160°W and leaving at 57°S, 140°W; the Eltanin Fracture Zone has the same orientation but lies approximately 5° to the north.

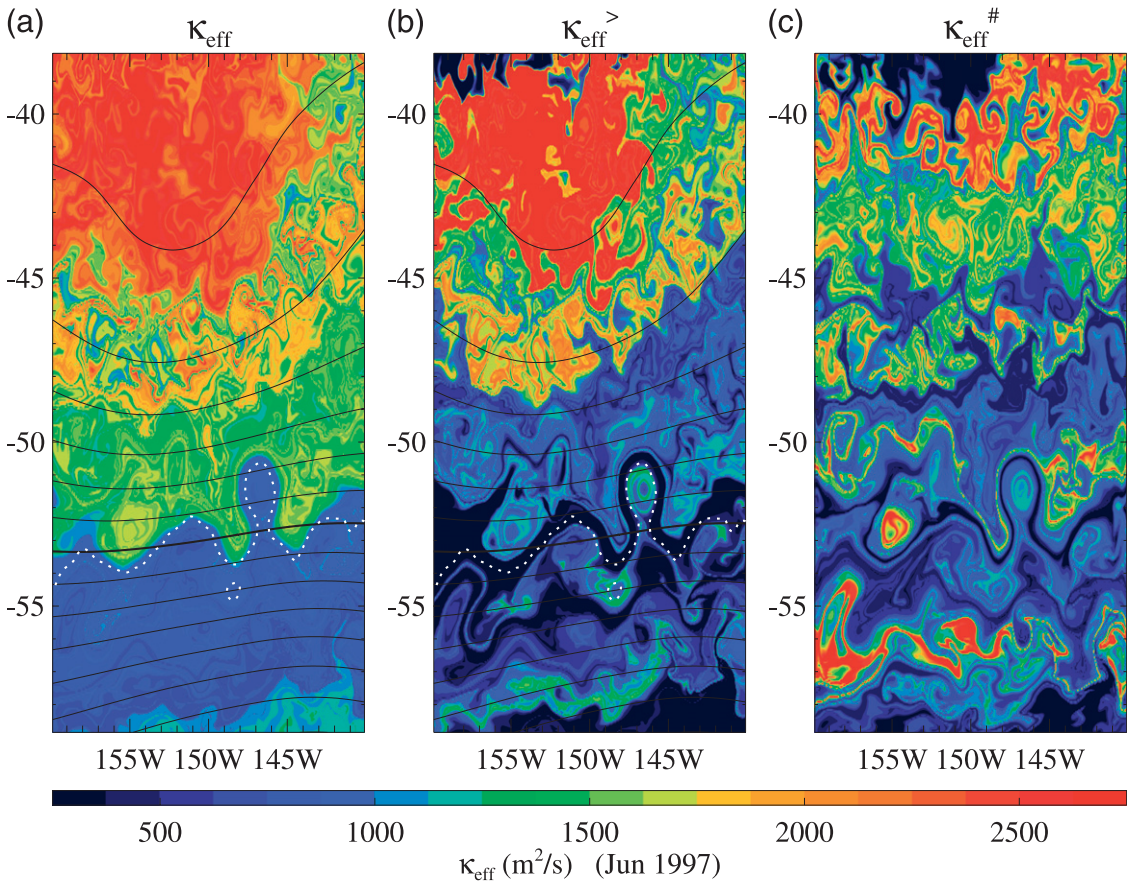

FIG. 3. Calculations of eddy diffusivity (a) κ_{eff}, (b) $\kappa_{eff}^{>}$, and (c) $\kappa_{eff}^{\#}$ in a patch of the Pacific on 28 Jun 1997. See text for details: effective diffusivity values (m^2 s^{-1}) in color; time-mean geostrophic streamfunction (black contours, zero contour bold, contour interval $\times 10^4$ m^2 s^{-1}); and the instantaneous geostrophic streamfunction (dotted white contour, only zero contour shown).

Moore et al. 1999). Indeed, jets are observed to pass along both the Udinstev and Eltanin Fracture Zones (Gille 1994; Hughes and Ash 2001). This is a region of strong EKE, and eddy mean–flow interactions are thought to play an important role in the dynamics (Hughes and Ash 2001). A maximum in Eady growth rate (see Williams et al. 2007; Fig. 7; Smith 2007) is indicative of baroclinic instability of the jet. However, perhaps surprisingly, this corresponds to a region of low values of effective diffusivity in Fig. 3 with the exception of the small regions of localized enhanced mixing in $\kappa_{eff}^{\#}$, which appears to be associated with the interior of the larger eddies. The eddy diffusivity calculations of Holloway (1986) and Stammer (1998) would, in contrast, predict this to be a region of large eddy diffusivity. To investigate this discrepancy, a calculation was performed where the velocity field was based solely on the SSH anomalies with no mean flow included. The results of the κ_{eff} calculation for this flow are presented in Fig. 4b. It can be seen that in this case the eddy diffusivity is, indeed, highest in the region of strong eddy kinetic energy within the ACC jet. The mean flow apparently plays an important role in suppressing mixing lengths and, hence, the eddy diffusivities in this region [see also Marshall et al. (2006) and Haynes et al. (2007)]. This likely explains why the calculations of Holloway (1986) and Stammer (1998), which do not contain explicit information about the mean flow, are in disagreement with those presented here (and indeed are closer to the results of the eddy diffusivity calculation for the velocity field with no mean flow). The eddy diffusivity results presented here help to explain the inverse modeling results of Gille (1999). These results indicated that the heat and salt carried by the ACC remain essentially unchanged as the current passes through regions of high eddy kinetic energy in this region, again in contrast to the predictions of Holloway (1986). It would be interesting to repeat the calculations here with an improved representation of the mean flow that better captured the influence of topography; this is left to a future study.

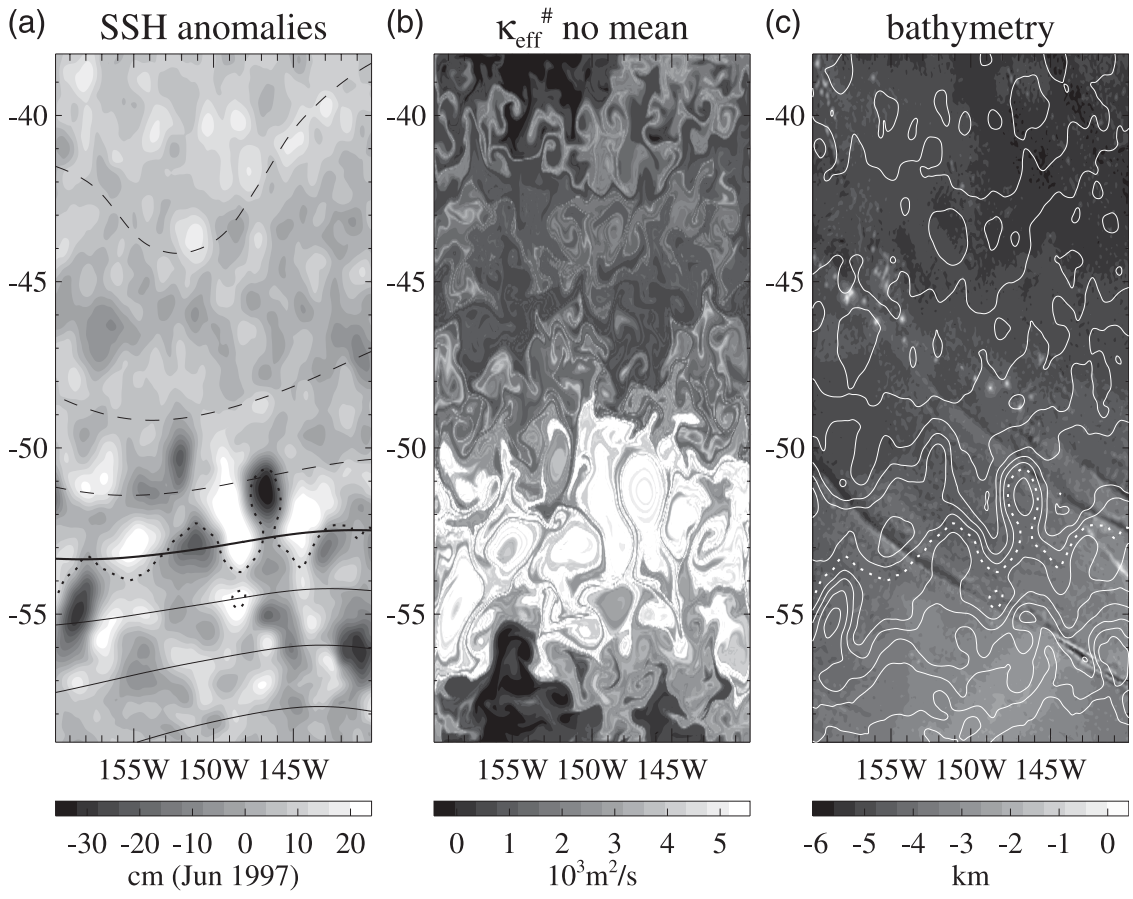

FIG. 4. (a) SSH anomalies from a patch of the Pacific on 28 Jun 1997 (contours as in Fig. 3); (b) κ_{eff} from a calculation where the velocity field is based solely on these anomalies, i.e., no mean flow has been included; and (c) bathymetry of this patch region with instantaneous streamlines overlaid.

The correspondence between jets and regions of small effective diffusivity (i.e., barriers to eddy mixing) at their cores with regions of large effective diffusivity (i.e., mixing regions) on their flanks has been noted before in the case of atmospheric flows (e.g., Haynes and Shuckburgh 2000a,b). Marshall et al. (2006) noted that regions of high effective diffusivity in the Southern Ocean coincide with regions of weak gradients in potential vorticity (PV), and those of low diffusivity with high potential vorticity gradient. More generally, the suppression of mixing at the centers of jets is a ubiquitous feature in geophysical fluid dynamics [see, e.g., the early studies of Juckes and McIntyre (1987) and Panetta (1993)]. Recently, Dritschel and McIntyre (2008) reviewed in detail the connection between the inhomogeneous mixing of PV in the presence of a background gradient and the presence of persistent jets in planetary atmospheres and oceans. They linked eddy-transport barriers to the Rossby wave elasticity that is concentrated at the barriers and, also, to the effects of shear straining of the collocated eastward jets (whose presence is dictated by PV inversion) and of the accompanying radiation-stress field (due, e.g., to momentum transport by Rossby waves). Other studies (Beron-Vera et al. 2008) have suggested that a kinematic effect arising from the theory of dynamical systems may be important in determining the barrier effect of jets.[4] McIntyre (2008) further emphasizes that Rossby waves propagating on the concentrated PV gradient at the jet core always have phase speeds with magnitude less than that of the mean flow and hence that there always exist critical lines on the jet flanks. This means that, whenever the jet is disturbed, it will be accompanied by irreversible mixing in the flanks to either side.

b. Chatham Rise

Figure 5 presents the results of the eddy diffusivity calculations in a patch of the Pacific, to the west of that

[4] See Haynes et al. (2007) for a discussion of transport and mixing in kinematic and dynamically consistent flows, and McIntyre (2008) for comments concerning natural and unnatural disturbances.

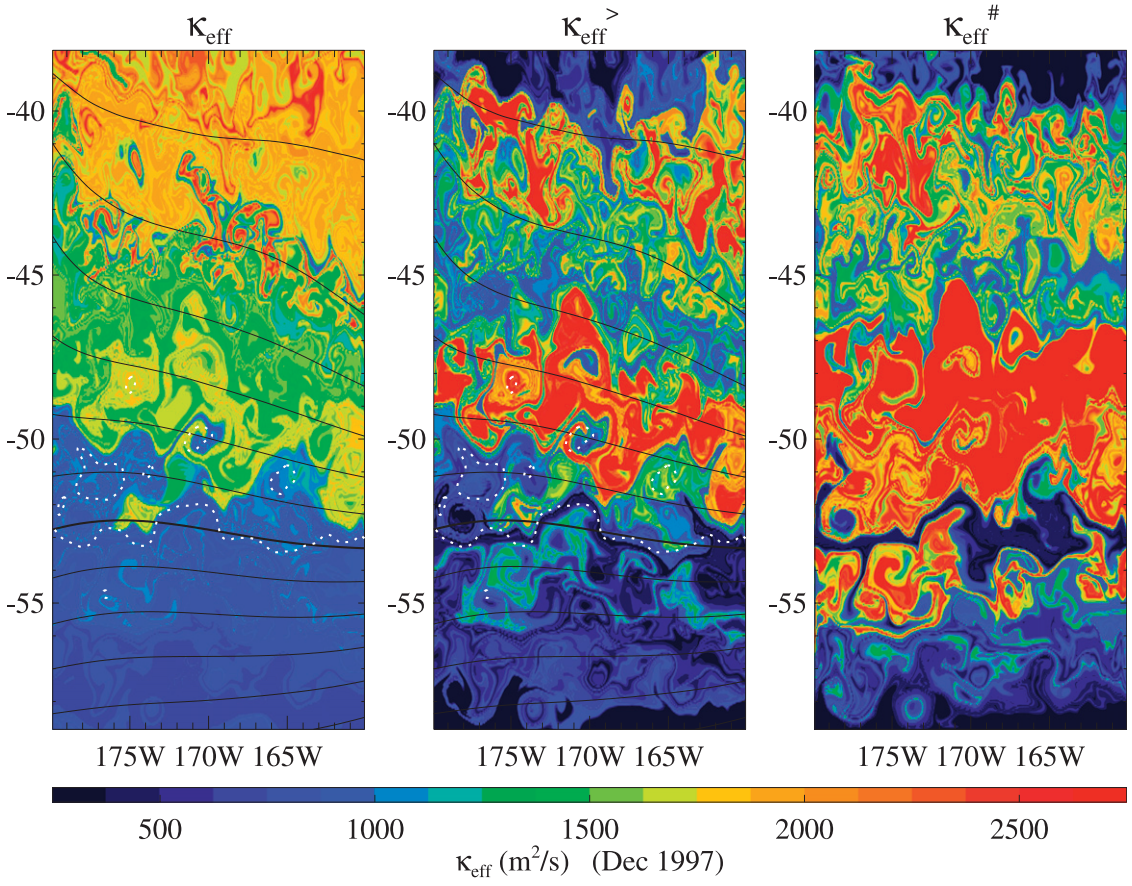

FIG. 5. Calculations of eddy diffusivity in a patch of the Pacific on 25 Dec 1997. See text for details. Effective diffusivity values ($m^2\ s^{-1}$) in color; time-mean geostrophic streamfunction (black contours, zero contour bold, contour interval $\times 10^4\ m^2\ s^{-1}$); and the instantaneous geostrophic streamfunction (dotted white contour, only zero contour shown).

in Fig. 3, from 38° to 59°S, 180° to 160°W. This patch is east of New Zealand, as can be seen from the bathymetry in Fig. 6c, where features associated with the Chatham Rise and Chatham Island (45°S, 176°W), Bounty Island (47°S, 179°E), and the Bollons Seamount (49.5°S, 176°W) are visible (white). The SSH anomalies indicate strongest eddy activity in a broad region south of 45°S, apparently less tightly associated with jets than in Fig. 4. The polar front is located significantly farther south than in the region of the Udinstev Fracture Zone, and south of the strongest EKE (see Hughes and Ash 2001). The strong eddy activity is likely to be a consequence of complex interactions with topography as the flow passes over the Campbell Plateau to the south of New Zealand (Bryden and Heath 1985). As in Fig. 3, the κ_{eff} is characterized by small values south of the patch and larger values to the north. The results of $\kappa^{>}_{\text{eff}}$ again show very low mixing associated with eastward jets in the flow (see, e.g., low $\kappa^{>}_{\text{eff}}$ associated with the zero streamline). Enhanced $\kappa^{>}_{\text{eff}}$ in the middle of the domain (around 50°S), not present in κ_{eff}, indicates that tracer structure is more complex in this region than at other longitudes. The results of the $\kappa^{\#}_{\text{eff}}$ calculation show even more enhanced values in this region, suggesting that much of the mixing is locally generated, presumably associated with the strong eddy activity in this region observed in Fig. 6a. The maximum values of $\kappa^{\#}_{\text{eff}}$ in this region fall around 48°S and reach values of more than $4000\ m^2\ s^{-1}$ (see also Fig. 8), consistent with the calculations of Sallée et al. (2008), confirming that the eddy diffusivity may play an important role in reducing the tendency for mixed layer destabilization in this region.

When we calculate $\kappa^{\#}_{\text{eff}}$ for the flow in this region with the mean flow removed (Fig. 6b), we find a pattern of high/low diffusivity that is rather similar to the case including the mean flow (although the absolute magnitude is increased). Why is there a correspondence in this region and not in the region 160°–140°W? The answer appears to lie in the interaction between the eddies and mean flow. It was suggested above that the explanation for the reduced eddy diffusivity in the neighborhood of high EKE for the Eltanin and Udinstev Fracture Zone

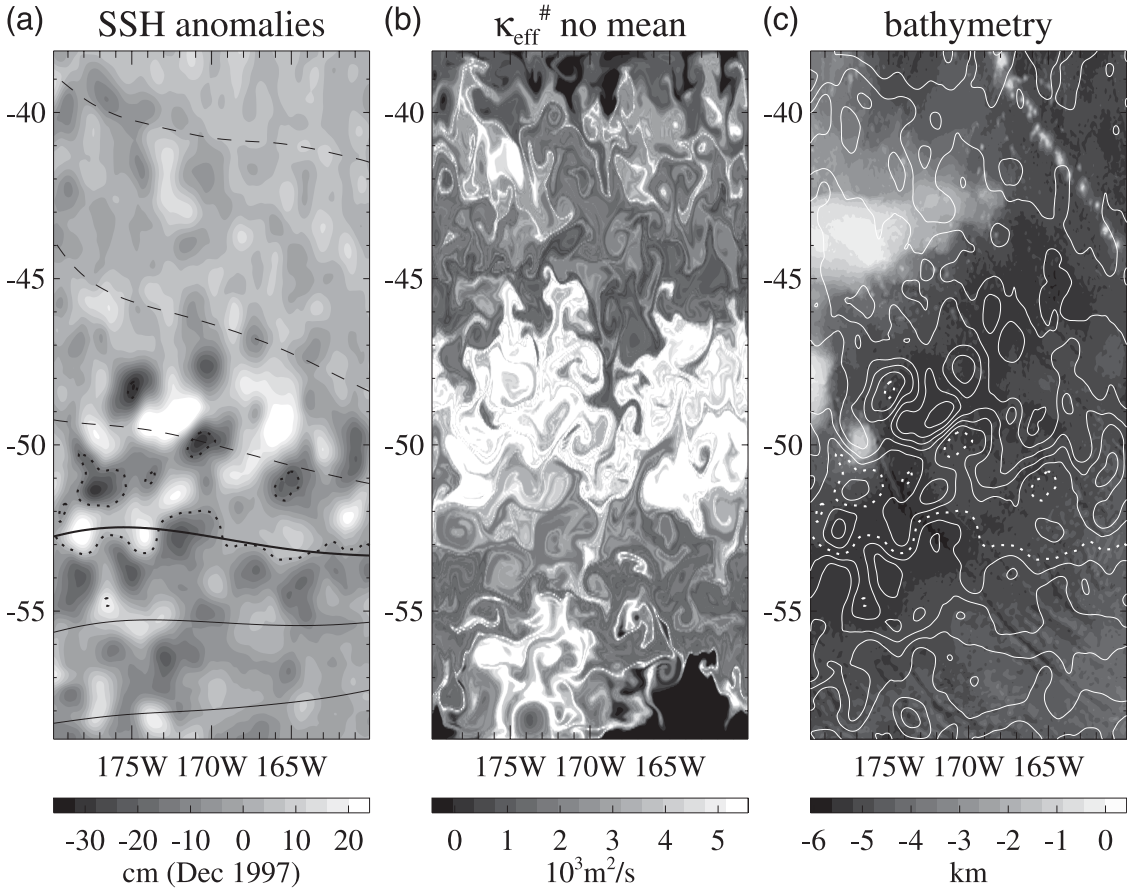

FIG. 6. (a) SSH anomalies from a patch of the Pacific on 25 Dec 1997 (contours as in Fig. 5); (b) κ_{eff} from a calculation where the velocity field is based solely on these anomalies, i.e., no mean flow has been included; and (c) bathymetry of this patch region with the instantaneous streamlines overlaid.

region is that the mean flow suppresses eddy diffusivity and the high EKE coincides with strong eastward jets. In the region of the Campbell Plateau, the strongest mean flow is to the south of the strongest eddy activity. Although this is a region of large EKE, the Eady growth rate is not large (Williams et al. 2007): the eddy activity is not obviously related to local instabilities of the mean flow. Instead, there is evidence that other mechanisms may be important: for example, it has been suggested (Chiswell and Sutton 1998) that eddies in this region may be formed by the separation of a frictional boundary layer at the eastern end of Chatham Rise (Bower et al. 1997; D'Asaro 1988). The offset between the region of strong eddy activity and strong mean flow allows the eddies to fully contribute to the eddy diffusivity.

c. Menard Fracture Zone

Figure 7a presents results of the eddy diffusivity calculations in a patch of the Pacific, to the east of that in Fig. 3, from 38° to 59°S, 120° to 100°W. This patch is in the vicinity of the East Pacific Rise, a ridge running approximately north–south. The Eltanin fracture, observed in Fig. 4, continues into this patch at around 56°S, and the Menard fracture enters the regions at around 50°S. The SSH anomalies (Fig. 7b) indicate significant eddy activity at about 55°S, but rather quiescent regions elsewhere. Correspondingly, the effective diffusivity $\kappa_{eff}^{\#}$ is rather weak everywhere except around 55°. It has been suggested by Shuckburgh et al. (2009b) that the eddy diffusivity is influenced by not only the EKE but also the mean zonal flow (u) and the phase speed of the eddies (c), scaling with the streamwise average of EKE/$(u - c)^2$. In Fig. 7c we therefore present these quantities (zonally averaged) for comparison with the effective diffusivity. The EKE broadly follows the same pattern of variability as κ_{eff}, with larger values south of the domain. However, there is also a clear influence on κ_{eff} of $(u - c)$: where this peaks at 55° and 58° there are correspondingly very low values of κ_{eff}.

d. Southeastern Pacific

Figure 8 continues to examine the relationship between $\kappa_{eff}^{\#}$, EKE, u, and c for other regions of the southeastern

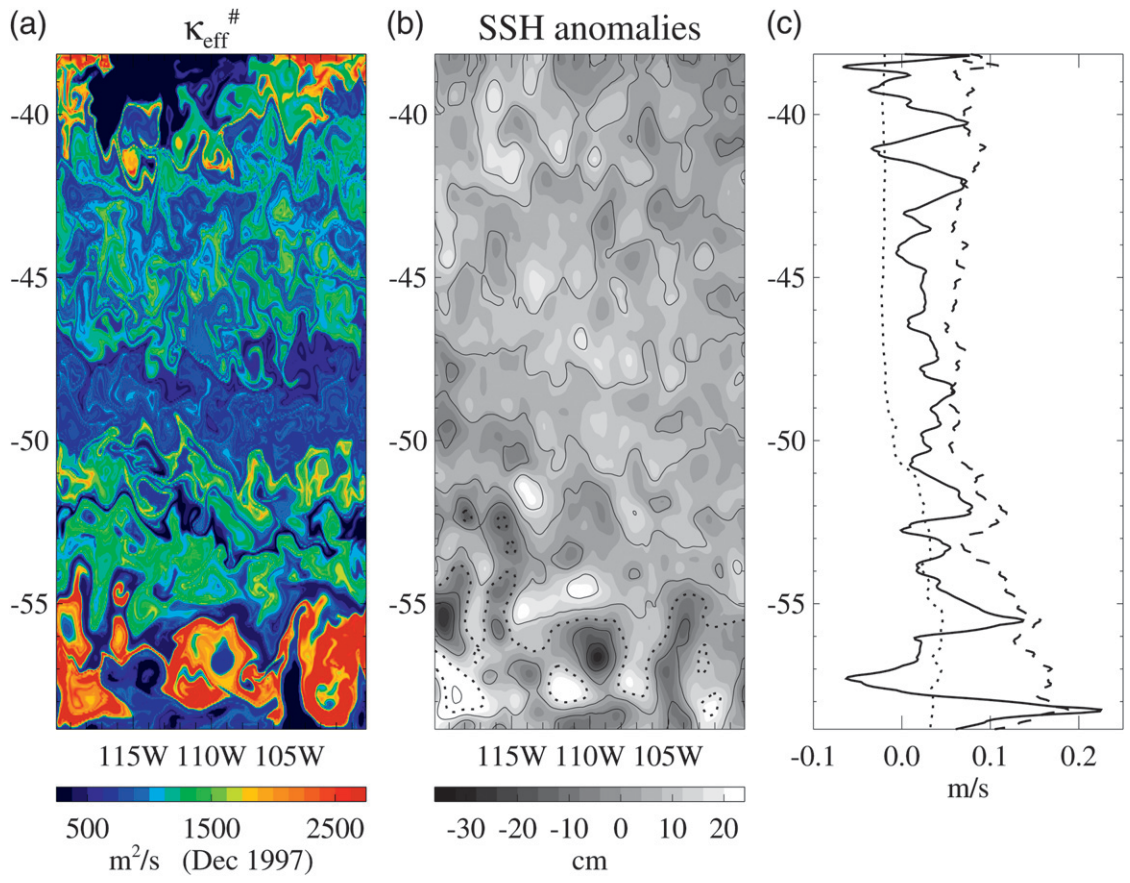

FIG. 7. (a) Calculations of the eddy diffusivity in a patch of the Pacific on 25 Dec 1997; $\kappa_{\text{eff}}^{\#}$ values in color. (b) SSH anomalies and the instantaneous geostrophic streamfunction (zero contour dotted). (c) Zonal means of the zonal velocity (u, solid), eddy kinetic energy ($\sqrt{\text{EKE}}$, dash), and phase speed of the eddies (c, dot). See text for details.

Pacific. For each sector there is broadly good agreement between $\sqrt{\text{EKE}}$ (black dash) and $\kappa_{\text{eff}}^{\#}$ calculated with no mean flow (blue). Looking to $\kappa_{\text{eff}}^{\#}$ (red), it can be seen that almost everywhere it is reduced in magnitude compared to the case with no mean flow (again, note the different scale) such that the typical value for the case with no mean flow is 2000–3000 $m^2\ s^{-1}$, whereas with the mean flow it is 1000 $m^2\ s^{-1}$. It can clearly be seen that where $(u - c)$ is small, $\kappa_{\text{eff}}^{\#}$ is large (e.g., 40°–45°S for both 180°–160°W and 160°–140°W; 48–49° and 55°S for 180°–160°W). Conversely, where $(u - c)$ is large, $\kappa_{\text{eff}}^{\#}$ is small (e.g., 52°–56°S, 160°–140°W and at 53°S, 180°–160°W). Over the deep ocean basin from 100° to 80°W all of the quantities are small at all latitudes. These results confirm that both EKE and $(u - c)$ contribute to the eddy diffusivity.

4. Seasonal variability of eddy diffusivity

Figure 7 presented results for 25 December 1997; Fig. 9 presents results for the same region, but six months earlier on 28 June 1997. The $\kappa_{\text{eff}}^{\#}$ values indicate significantly more mixing in June equatorward of 45°S and less mixing poleward of 55°S. Looking to panel c in each figure, it can be seen that poleward of 55°S EKE (dash) is smaller in June (Fig. 9) than in December (Fig. 7) and the zonal velocity exhibits more westerly jets. The strongest mixing seen in $\kappa_{\text{eff}}^{\#}$ is confined to the region around 56°S where the eddy activity is large, but the zonal velocities are weak. Equatorward of 45°S it is more difficult to discern any systematic differences between June and December for either EKE or $(u - c)$, suggesting that variations in the eddy diffusivity can arise through rather subtle interactions between the eddy field and mean flow.

The temporal variability is examined further in Fig. 10. The $\kappa_{\text{eff}}^{\#}$ results are plotted from the start of the tracer integration on 30 December 1996 for a full year. The results from the first three months are during the spinup period and so should be treated with caution. For the 160°–140°W sector, the region equatorward of 45°S is a region of apparently larger eddy diffusivity during the late winter (July–September) than in summer. A region of very weak eddy diffusivity is present throughout the

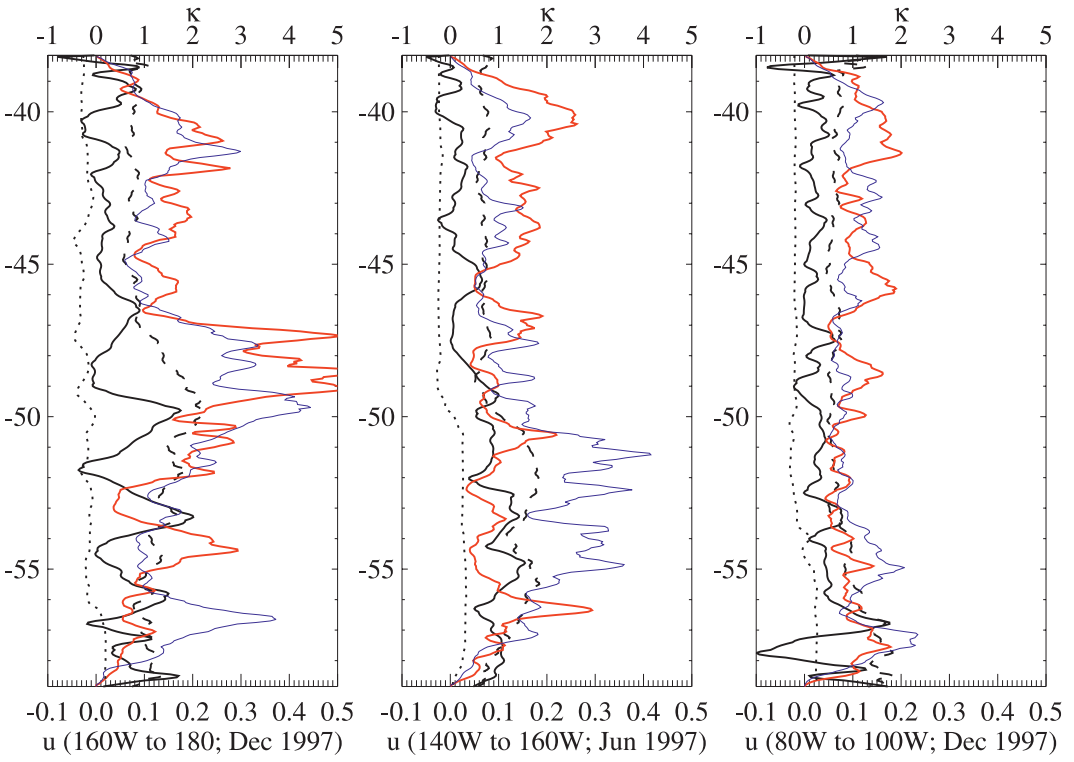

FIG. 8. Zonal means of the zonal velocity (u, black solid), eddy kinetic energy ($\sqrt{\text{EKE}}$, black dashed), and phase speed of the eddies (c, black dot); all in m s^{-1}: $\kappa^{\#}_{\text{eff}}$ ($\times 10^3$ m^2 s^{-1}, red) and $\kappa^{\#}_{\text{eff}}$ calculated with no mean flow ($\times 2000$ m^2 s^{-1}, blue).

year at approximately 47°S, associated with a jet in the zonal mean flow. Poleward of this, there is significant variability both in the zonal mean flow and in the eddy diffusivity. The jets in this region, which are not tied to topography as the flow moves into the deep ocean basin, are known to migrate significantly in time (Moore et al. 1999). Consistent with our findings that the mean flow is a significant contributor to the eddy diffusivity, it can be seen clearly that for the sectors 180°–160°W and 160°–140°W, weak mean flow is frequently associated with strong eddy diffusivity, and vice versa, with changes in the mean flow often (but not always) being associated with changes in the eddy diffusivity.

5. Conclusions and discussion

This paper has introduced a framework for investigating the along-stream variability of the cross-stream eddy diffusivity. The sector of the Southern Ocean in the Pacific from 180° to 80°W has been chosen for particular examination; however, the framework could equally be applied to other regions of the oceans.

The regional calculations have highlighted some locally enhanced mixing in the ACC region, collocated with features in the bottom topography. The strongest jets are typically associated with reduced eddy diffusivities, and more generally the eddy diffusivity is seen to be reduced in the presence of a strong mean flow. Conversely, where the mean flow is displaced with respect to the strongest eddy activity, such as to the east of New Zealand, the eddy diffusivity is much larger. One of the important conclusions of these regional calculations is that the eddy kinetic energy (and, by implication, measures based directly on sea surface height anomalies) is not always a good guide to the magnitude of the eddy diffusivity quantified here. Previous studies (e.g., Jayne and Marotzke 2002) have noted that the eddy kinetic energy may not be a good measure of the eddy diffusivity where there is a coherent meandering jet. Here we note that, even in regions where baroclinic instability is thought to dominate, the mean flow can significantly suppress the eddy diffusivity. Moreover, analysis of seasonal variability indicates that the interaction between the eddy field and mean flow can be subtle and lead to significant changes in the eddy diffusivity.

The dependence of the eddy diffusivity on both the mean flow[5] and eddy kinetic energy is highlighted in

[5] The phase speed c of the eddies is small throughout the Pacific region of the Southern Ocean, so we chose here to plot u rather than $u - c$ since the results are less noisy.

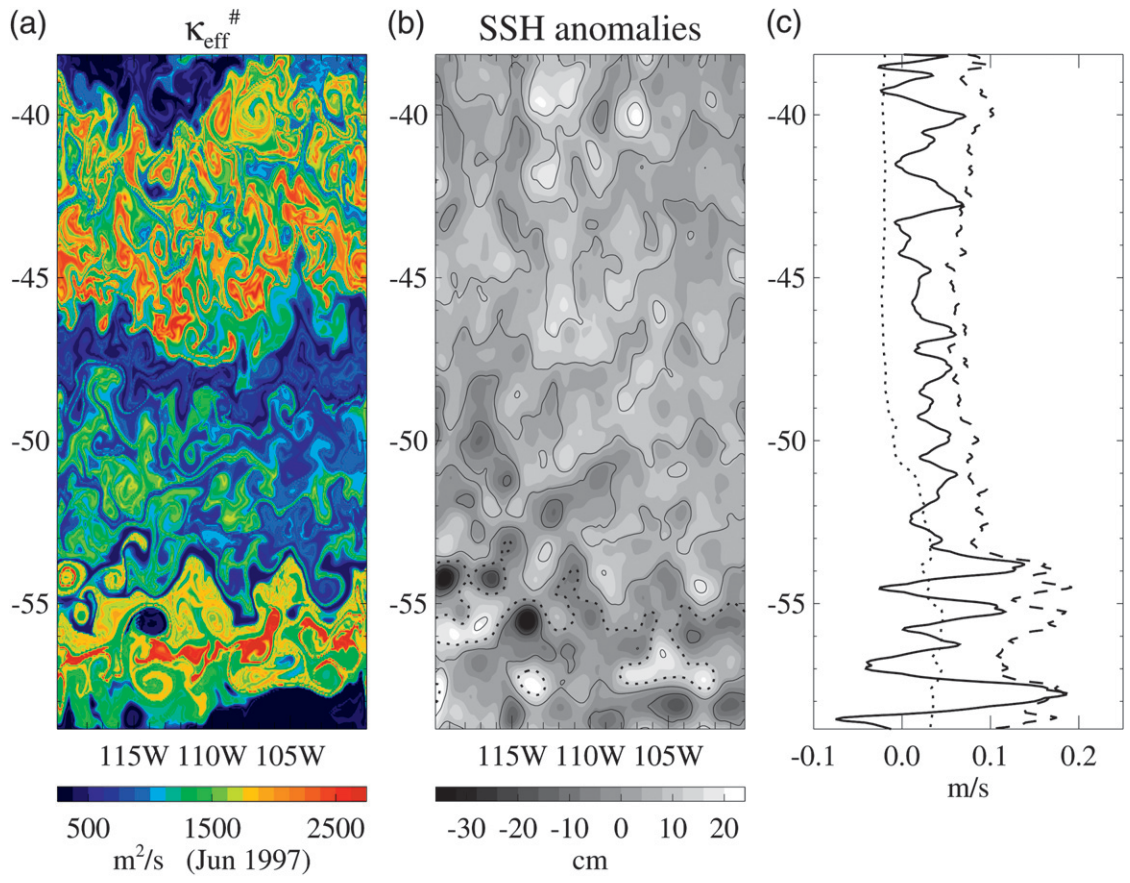

FIG. 9. (a) Calculations of eddy diffusivity in a patch of the Pacific on 28 Jun 1997; effective diffusivity values in color; (b) SSH anomalies and the instantaneous geostrophic streamfunction (zero contour dotted); and (c) zonal means of the zonal velocity (u, solid), eddy kinetic energy ($\sqrt{\text{EKE}}$, dash), and phase speed of the eddies (c, dot). See text for details.

Fig. 11. It can be seen that, in broad terms, with relatively strong mean eastward flow and relatively weak eddy kinetic energy (above the dashed line) there is a tendency for small values of eddy diffusivity (blue points), whereas for relatively weak mean flow and strong eddy kinetic energy (below the dashed line) there is a tendency for large values of eddy diffusivity (red points). It can be seen further that there are two groupings of large values of eddy diffusivity in Fig. 11: one equatorward of the ACC (red circles) with small values of zonal mean velocity and relatively small values of eddy kinetic energy and the other in the region of the ACC (red squares) with relatively large values of eddy kinetic energy and a range of values of the zonal mean flow. There are also two groupings of small values of eddy diffusivity (blue points): one for moderate values of eddy kinetic energy ($\sqrt{\text{EKE}} = 0.1\ \text{m s}^{-1}$), which arises from the region of stronger eddy activity on the western side of the region under consideration, the other for small values of eddy kinetic energy ($\sqrt{\text{EKE}} = 0.07\ \text{m s}^{-1}$), which arises from the more quiescent region on the eastern side of the Pacific.

Shuckburgh et al. (2009b) found that the spatial and temporal variability of eddy diffusivity in the Southern Ocean is related to the streamwise-average EKE/$(u - c)^2$. The results here suggest that this relationship also holds regionally, at least in the Pacific sector of the Southern Ocean. Following a framework based on potential vorticity, the weak mixing where the mean flow is strong is thought to be associated with the barrier effect generated by Rossby wave elasticity and shear straining at eastward jets (Dritschel and McIntyre 2008), and the strong mixing where the eddy kinetic energy is large is thought to be associated with Rossby wave breaking near critical layers where the phase speed of the wave equals the mean zonal flow (McIntyre 2008).

One of the attractions of using the effective diffusivity diagnostic described here is that it is by definition related to the evolution of a tracer field. Alternative measures of eddy mixing based on Lagrangian particles can lead to quite different results, particularly in terms of regional variability. For example, calculation of Lagrangian stretching rates using surface geostrophic

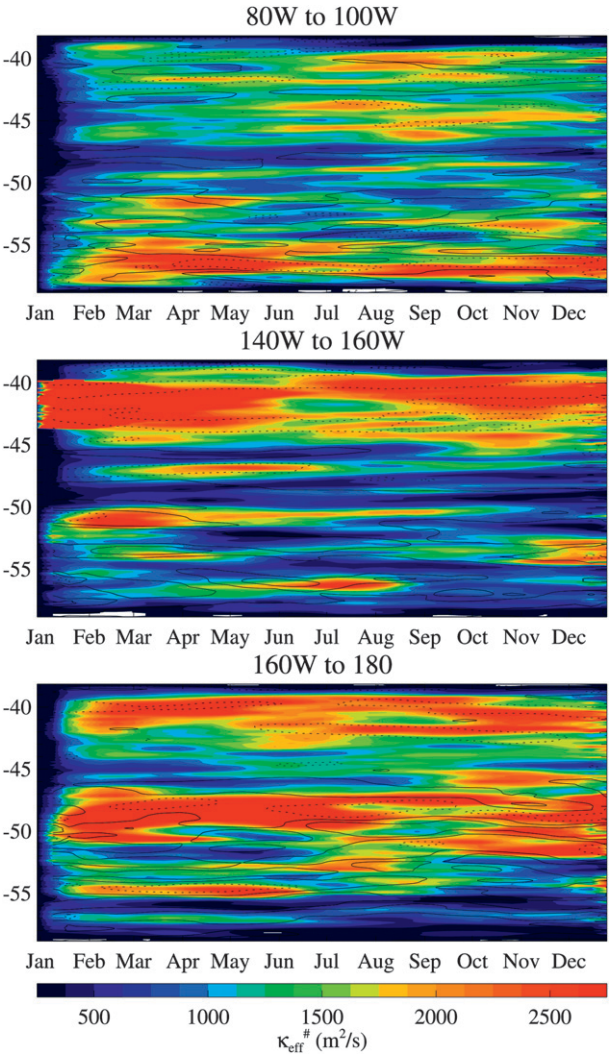

FIG. 10. Time dependence of $\kappa^{\#}_{\text{eff}}$ for three sectors with zonal-mean zonal velocity overlaid (zero contour dotted).

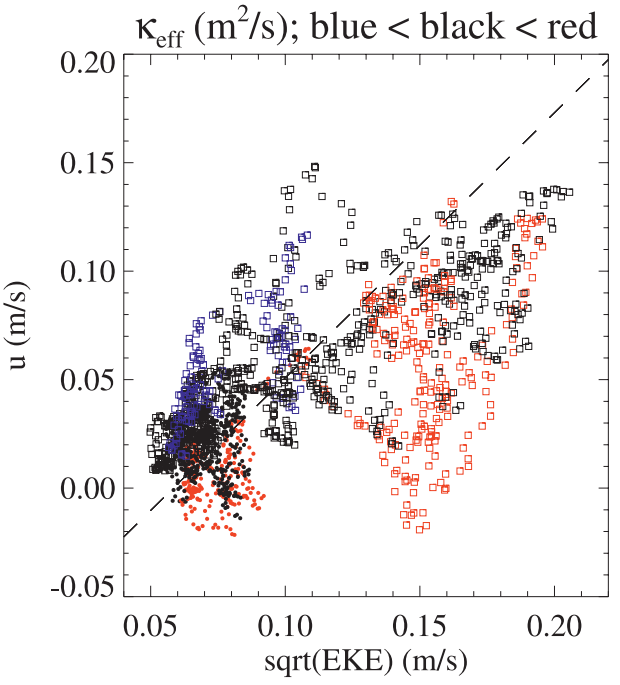

FIG. 11. Dependence of $\kappa^{\#}_{\text{eff}}$ on mean flow u and eddy kinetic energy $\sqrt{\text{EKE}}$. Time and zonal averages taken for each of the five Pacific patches: $\kappa^{\#}_{\text{eff}} < 800$, blue; $800 < \kappa^{\#}_{\text{eff}} < 1600$, black; $\kappa^{\#}_{\text{eff}} > 1600$, red; in $\text{m}^2\ \text{s}^{-1}$. Points equatorward of the ACC from 47° to 39°S are plotted as filled circles, in the ACC region from 58° to 47°S as squares. The dashed line highlights the different regimes.

currents derived from altimetry reveals a close correspondence with the EKE (Waugh et al. 2006). Analysis of float trajectories (e.g., Sallée et al. 2008) provides Lagrangian statistics with a regional variability that is also more akin to the EKE. It would be helpful to be able to reconcile these Lagrangian-particle-based measures with the effective diffusivity. It may be possible to achieve this by applying the approach of d'Ovidio et al. (2009; Shuckburgh 2009a), which combines aspects of both tracer and particle diagnostics to form a Lyapunov diffusivity.

Finally, the approach outlined in this paper may be helpful both for developing and testing eddy parameterizations. The subtle relationship between the eddy field and mean flow, which varies from region to region, provides a challenge to eddy parameterization schemes if they are to accurately reproduce the eddy influence on the overturning circulation and ACC transport (Hallberg and Gnandesikan 2006; Treguier et al. 2007). Certainly the results presented here and in Shuckburgh et al. (2009b) cast doubt on the ability of parameterizations based solely on the eddy kinetic energy (Eden and Greatbatch 2008) to accurately represent the eddy diffusivity in regions of strongly varying mean flow such as the Southern Ocean.

Acknowledgments. EFS would like to thank Mike Meredith, Raffaele Ferrari, and Darryn Waugh for helpful discussions. EFS is supported by a Natural Environment Research Council fellowship. JM acknowledges the support of the National Science Foundation (Polar Program). The comments of two anonymous reviewers were very helpful in improving the manuscript.

REFERENCES

Beron-Vera, F. J., M. G. Brown, M. J. Olascoaga, I. I. Rypina, H. Kocak, and I. A. Udovydchenkov, 2008: Zonal jets as transport barriers in planetary atmospheres. *J. Atmos. Sci.,* **65,** 3316–3326.

Bower, A. S., L. Armi, and I. Ambar, 1997: Lagrangian observations of meddy formation during a Mediterranean undercurrent seeding experiment. *J. Phys. Oceanogr.,* **27,** 2545–2575.

Bryden, H. L., and R. A. Heath, 1985: Energetic eddies at the northern edge of the Antarctic circumpolar current in the southwest Pacific. *Prog. Oceanogr.,* **14,** 65–87.

Chiswell, S. M., and P. J. H. Sutton, 1998: A deep eddy in the Antarctic Intermediate Water north of Chatham Rise. *J. Phys. Oceanogr.,* **28,** 535–540.

D'Asaro, E. A., 1988: Generation of submesoscale vortices: A new mechanism. *J. Geophys. Res.,* **93,** 6685–6691.

d'Ovidio, F., E. Shuckburgh, and B. Legras, 2009: Local mixing events in the upper troposphere and lower stratosphere. Part I: Detection with the Lyapunov diffusivity. *J. Atmos. Sci.,* in press.

Dritschel, D. G., and M. E. McIntyre, 2008: Multiple jets as PV staircases: The Phillips effect and the resilience of eddy-transport barriers. *J. Atmos. Sci.,* **65,** 855–874.

Eden, C., and R. J. Greatbatch, 2008: Towards a mesoscale eddy closure. *Ocean Modell.,* **20,** 223–239.

Gille, S. T., 1994: Mean sea surface height of the Antarctic circumpolar current from Geosat data: Method and application. *J. Geophys. Res.,* **99,** 18 255–18 273.

——, 1997: The Southern Ocean momentum balance: Evidence for topographic effects from numerical model output and altimeter data. *J. Phys. Oceanogr.,* **27,** 2219–2232.

——, 1999: Mass, heat, and salt transport in the southeastern Pacific: A circumpolar current inverse model. *J. Geophys. Res.,* **104,** 5191–5209.

Hallberg, R., and A. Gnandesikan, 2001: An exploration of the role of transient eddies in determining the transport of a zonally reentrant current. *J. Phys. Oceanogr.,* **31,** 3312–3330.

——, and ——, 2006: The role of eddies in determining the structure and response of the wind-driven Southern Hemisphere overturning: Results from the Modeling Eddies in the Southern Ocean (MESO) project. *J. Phys. Oceanogr.,* **36,** 2232–2252.

Haynes, P. H., and E. F. Shuckburgh, 2000a: Effective diffusivity as a diagnostic of atmospheric transport, 1. Stratosphere. *J. Geophys. Res.,* **105,** 22 777–22 794.

——, and ——, 2000b: Effective diffusivity as a diagnostic of atmospheric transport, 2. Troposphere and lower stratosphere. *J. Geophys. Res.,* **105,** 22 795–22 810.

——, D. A. Poet, and E. F. Shuckburgh, 2007: Transport and mixing in kinematic and dynamically consistent flows. *J. Atmos. Sci.,* **64,** 3640–3651.

Holloway, G., 1986: Estimation of oceanic eddy transports from satellite altimetry. *Nature,* **323,** 243–244.

Hughes, C., and E. Ash, 2001: Eddy forcing of the mean flow in the Southern Ocean. *J. Geophys. Res.,* **106,** 2713–2772.

Jayne, S. R., and J. Marotzke, 2002: Oceanic eddy heat transport. *J. Phys. Oceanogr.,* **32,** 3328–3345.

Juckes, M. N., and M. E. McIntyre, 1987: A high resolution, one-layer model of breaking planetary waves in the stratosphere. *Nature,* **328,** 590–596.

Karsten, R., and J. Marshall, 2002: Constructing the residual circulation of the ACC from observations. *J. Phys. Oceanogr.,* **32,** 3315–3327.

Keffer, T., and G. Holloway, 1988: Estimating Southern Ocean eddy flux of heat and salt from satellite altimetry. *Nature,* **332,** 624–626.

Lenn, Y. D., T. K. Chereskin, J. Sprintall, and E. Firing, 2007: Mean jets, mesoscale variability and eddy momentum fluxes in the surface layer of the Antarctic Circumpolar Current in Drake Passage. *J. Mar. Res.,* **65,** 27–58.

Marshall, J., and T. Radko, 2003: Residual-mean solutions for the Antarctic Circumpolar Current and its associated overturning circulation. *J. Phys. Oceanogr.,* **33,** 2341–2354.

——, A. Adcroft, C. Hill, L. Perelman, and C. Heisey, 1997: A finite-volume, incompressible Navier–Stokes model for studies of the ocean on parallel computers. *J. Geophys. Res.,* **102,** 5753–5766.

——, E. Shuckburgh, H. Jones, and C. Hill, 2006: Estimates and implications of surface eddy diffusivity in the Southern Ocean derived from tracer transport. *J. Phys. Oceanogr.,* **36,** 1806–1821.

McIntyre, M. E., 2008: Potential-vorticity inversion and the wave-turbulence jigsaw: Some recent clarifications. *Adv. Geosci.,* **15,** 47–56.

Moore, J. K., M. R. Abbott, and J. G. Richman, 1999: Location and dynamics of the Antarctic polar front from satellite sea surface temperature data. *J. Geophys. Res.,* **104,** 3059–3073.

Nakamura, N., 1996: Two-dimensional mixing, edge formation, and permeability diagnosed in area coordinates. *J. Atmos. Sci.,* **53,** 1524–1537.

Panetta, R. L., 1993: Zonal jets in wide baroclinically unstable regions: Persistence and scale selection. *J. Atmos. Sci.,* **50,** 2073–2106.

Rhines, P. B., 1975: Waves and turbulence on a beta-plane. *J. Fluid Mech.,* **69,** 417–443.

Sallée, J., K. Speer, R. A. Morrow, and R. Lumpkin, 2008: An estimate of Lagrangian eddy statistics and diffusion in the mixed layer of the Southern Ocean. *J. Mar. Res.,* **66,** 441–463.

Shuckburgh, E., and P. Haynes, 2003: Diagnosing transport and mixing using a tracer-based co-ordinate system. *Phys. Fluids,* **15,** 3342–3357.

——, W. Norton, A. Iwi, and P. Haynes, 2001: Influence of the quasi-biennial oscillation on isentropic transport and mixing in the tropics and subtropics. *J. Geophys. Res.,* **106,** 14 327–14 337.

——, F. d'Ovidio, and B. Legras, 2009a: Local mixing events in the upper troposphere and lower stratosphere. Part II: Seasonal and interannual variability. *J. Atmos. Sci.,* in press.

——, H. Helen, J. Marshall, and C. Hill, 2009b: Robustness of an effective diffusivity diagnostic in oceanic flows. *J. Phys. Oceanogr.,* **39,** 1993–2009.

Smith, K. S., 2007: The geography of linear baroclinic instability in Earth's oceans. *J. Marine Res.,* **65,** 655–683.

Smith, W., and D. Sandwell, 1997: Global seafloor topography from satellite altimetry and ship depth soundings. *Science,* **227,** 1957–1962.

Sokolov, S., and S. R. Rintoul, 2007: Multiple jets of the Antarctic Circumpolar Current south of Australia. *J. Phys. Oceanogr.,* **37,** 1394–1412.

Stammer, D., 1997: Global characteristics of ocean variability estimated from regional TOPEX/Poseidon altimeter measurements. *J. Phys. Oceanogr.,* **27,** 1743–1769.

——, 1998: On eddy characteristics, eddy transports, and mean flow properties. *J. Phys. Oceanogr.,* **28,** 727–739.

——, C. Wunsch, and K. Ueyoshi, 2006: Temporal changes in ocean eddy transports. *J. Phys. Oceanogr.,* **36,** 543–550.

Treguier, A. M., M. H. England, S. R. Rintoul, G. Madec, J. Le Sommer, and J. M. Molines, 2007: Southern Ocean overturning across streamlines in an eddying simulation of the Antarctic Circumpolar Current. *Ocean Sci.,* **3,** 491–507.

Waugh, D., E. Abraham, and M. Bowen, 2006: Spatial variations of stirring in the surface ocean: A case study of the Tasman Sea. *J. Phys. Oceanogr.,* **36,** 526–542.

Williams, R. G., C. Wilson, and C. W. Hughes, 2007: Ocean and atmosphere storm tracks: The role of eddy vorticity forcing. *J. Phys. Oceanogr.,* **37,** 2267–2289.